Inorganic Chemistry

Article

pubs.acs.org/IC

Luminescence and Energy Transfer Properties of $Ca_2Ba_3(PO_4)_3Cl$ and $Ca_2Ba_3(PO_4)_3Cl$:A (A = Eu^{2+}/Ce^{3+}/Dy^{3+}/Tb^{3+}) under UV and Low-Voltage Electron Beam Excitation

Mengmeng Shang,[†,‡] Dongling Geng,[†,‡] Dongmei Yang,[†,‡] Xiaojiao Kang,[†,‡] Yang Zhang,[†,‡] and Jun Lin*[,†]

[†]State Key Laboratory of Rare Earth Resource Utilization, Changchun Institute of Applied Chemistry, Chinese Academy of Sciences, Changchun 130022, P. R. China

[‡]University of Chinese Academy of Sciences, Beijing 100049, P. R. China

Supporting Information

ABSTRACT: Pure $Ca_2Ba_3(PO_4)_3Cl$ and rare earth ion (Eu^{2+}/Ce^{3+}/Dy^{3+}/Tb^{3+}) doped $Ca_2Ba_3(PO_4)_3Cl$ phosphors with the apatite structure have been prepared via a Pechini-type sol−gel process. X-ray diffraction (XRD) and structure refinement, photoluminescence (PL) spectra, cathodoluminescence (CL) spectra, absolute quantum yield, as well as lifetimes were utilized to characterize samples. Under UV light excitation, the undoped $Ca_2Ba_3(PO_4)_3Cl$ sample shows broad band photoluminescence centered near 480 nm after being reduced due to the defect structure. Eu^{2+} and Ce^{3+} ion doped $Ca_2Ba_3(PO_4)_3Cl$ samples also show broad 5d → 4f transitions with cyan and blue colors and higher quantum yields (72% for $Ca_2Ba_3(PO_4)_3Cl$:0.04Eu^{2+}; 67% for $Ca_2Ba_3(PO_4)_3Cl$:0.016Ce^{3+}). For Dy^{3+} and Tb^{3+} doped $Ca_2Ba_3(PO_4)_3Cl$ samples, they give strong line emissions coming from 4f → 4f transitions. Moreover, the Ce^{3+} ion can transfer its energy to the Tb^{3+} ion in the $Ca_2Ba_3(PO_4)_3Cl$ host, and the energy transfer mechanism has been demonstrated to be a resonant type, via a dipole−quadrupole interaction. However, under the low voltage electron beam excitation, Tb^{3+} ion doped $Ca_2Ba_3(PO_4)_3Cl$ samples present different luminescence properties compared with their PL spectra, which is ascribed to the different excitation mechanism. On the basis of the good PL and CL properties of the $Ca_2Ba_3(PO_4)_3Cl$:A (A = Ce^{3+}/Eu^{2+}/Tb^{3+}/Dy^{3+}), $Ca_2Ba_3(PO_4)_3Cl$ might be promising for application in solid state lighting and field-emission displays.

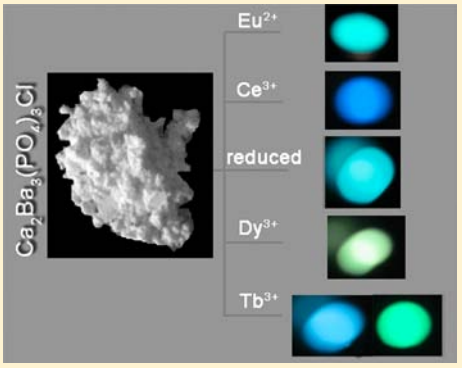

INTRODUCTION

Inorganic luminescent materials/phosphors are playing a key role in applications of lighting (e.g., fluorescent tubes and LEDs), displays (e.g., cathode tube display and field emission display), imaging (computed tomography), etc.[1−4] The current attention on energy savings and green issues gives a boost to the development of LEDs for lighting, due to their advantages of high efficiency, compactness, long operational lifetime, and environmental friendliness.[2,3] More importantly, LEDs have already entered the market as backlights for liquid crystal displays, replacing fluorescent lamps. Moreover, in the display field, although LCDs have a great market at present, FEDs have applications in some specific areas, such as special military devices, besides the general flat display applications. FEDs have the potential to provide displays with thin panels, self-emission, wide viewing, quick response times, high brightness, a high contrast ratio, light weight, and low power consumption. So LEDs and FEDs have attracted great interest from researchers, and searching for appreciate FED phosphors has been a hot topic.

One type of phosphor is based on an optically inactive host lattice into which activator ions are doped in small and optimized concentrations, typically a few mole percent or less. These activator ions have excitation energy levels that can be populated by direct excitation or indirectly by energy transfer, and emissions from these states are subsequently observed. Rare earth ions have been playing an important role in this type of phosphor due to the abundant emission colors based on their 4f → 4f or 5d → 4f transitions.[5,6] Such a phosphor, when appropriately activated, emits radiation in a narrow frequency range ("line emission") of the visible light spectrum, unlike an incandescent filament that emits over the full spectral range, though not all colors equally. The narrow line emission is due to the fact that optical activator ions (most trivalent rare earth ions and Ce^{3+} as the major exception) have a weak coupling with the host lattice, and the transitions between their 4f terms will be well shielded. However, Eu^{2+} and Ce^{3+} ions are the major rare earth ions with broad band emitting due to the 5d excited state. A different type of phosphor relies for its photoluminescence on the creation of electron−hole pairs within specific sites or clusters in a lattice without the presence

Received: November 25, 2012
Published: March 6, 2013

   dx.doi.org/10.1021/ic3025759 | Inorg. Chem. 2013, 52, 3102−3112

of doped activators. Here, electronic states created between the valence and conduction bands are defect-induced, and broad emission bands are the consequence of different chemical bonding environments in the ground and excited state.[7,8]

In this work, we present a novel kind of luminescent material with the general composition of $Ca_2Ba_3(PO_4)_3Cl$:A (A = Eu^{2+}, Ce^{3+}, Tb^{3+}, Dy^{3+}), which can be excited by UV light and a low voltage electron beam. Under our experimental synthesis conditions, the undoped $Ca_2Ba_3(PO_4)_3Cl$ sample reduced in the N_2/H_2 gas mixture shows a self-activated broad band emission ranging from 350 to 600 nm when excited in the far-UV region near 254 nm. Moreover, the $Ca_2Ba_3(PO_4)_3Cl$ host lattice shows the corresponding broad band and line emissions when doped with rare earth activators (Eu^{2+}, Ce^{3+}, Tb^{3+}, or Dy^{3+} ion). We also investigated the photoluminescence (PL) and cathodoluminescence (CL) properties as well as the energy transfer phenomenon between Ce^{3+} and Tb^{3+} in detail.

EXPERIMENTAL SECTION

Chemicals and Materials. The rare-earth oxides, including Eu_2O_3, Tb_4O_7, Dy_2O_3, and $Ce_2(CO_3)_2$ (all with purity of 99.999%), were purchased from the Science and Technology Parent Company of Changchun Institute of Applied Chemistry. A colorless stock solution of $Ln(NO_3)_3$ (Ln = Eu, Tb, Dy, Ce) with a certain concentration was prepared by dissolving the corresponding rare-earth oxides in dilute HNO_3. Other chemicals were purchased from Beijing Chemical Company. All chemicals were analytical grade reagents and used directly without further purification.

Preparation. The $Ca_2Ba_3(PO_4)_3Cl$:xEu^{2+}/yCe^{3+}/zTb^{3+}/mDy^{3+} ($0 \le x, y, z \le 0.20$; $0 \le m \le 0.05$) samples were all prepared by the Pechini-type sol–gel method.[7] The Ce^{3+}, Eu^{2+}, Tb^{3+}, and Dy^{3+} ions substitute for Ca^{2+} in the $Ca_2Ba_3(PO_4)_3Cl$ host, and x, y, z, and m are all given in mole percent. Typically, stoichiometric amounts of $Ln(NO_3)_3$ solution, $CaCl_2$, and $BaCl_2{\cdot}2H_2O$ were mixed in deionized water under stirring. The citric acid was dissolved in the above solution (citric acid/metal ion = 2:1 in moles). The pH of the solution was adjusted to a low value with HNO_3 followed by the addition of a stoichiometric amount of $(NH_4)H_2PO_4$. Finally, a certain amount of polyethylene glycol (PEG, molecular weight = 10 000) was added as a cross-linking agent. The citric acid is used to form stable metal complexes, and its polyesterification with a polyethylene glycol (PEG) forms a polymeric resin. Immobilization of metal complexes in such rigid organic polymer networks reduces the segregation of particular metal ions, ensuring compositional homogeneity.[9] The resultant mixtures were stirred for 1 h and heated at 75 °C in a water bath until homogeneous gels formed. After being dried in an oven at 110 °C for 10 h, the gels were ground and prefired at 500 °C in the air for 4 h. Then, the mixtures were fully ground and first sintered at 1000 °C for 4 h in the air, then reduced for 3 h under a 10% H_2/90% N_2 gas mixture at 800 °C. Finally, the as-synthesized samples were slowly cooled to room temperature inside the tube furnace under a H_2–N_2 flow

Characterization. The composition and phase purity of products were studied with X-ray powder diffraction (XRD) measurements using a D8 Focus diffractometer (Bruker) with Cu Kα radiation (λ = 0.15405 nm). The data were collected over a 2θ range from 10° to 120° at intervals of 0.02° with a counting time of 2 s per step. Structure refinements of X-ray diffractograms were made using the GSAS (general structure analysis system) program.[10] The morphology of the samples was inspected using a field-emission scanning electron microscope (FE-SEM, S-4800, Hitachi). Transmission electron microscopy (TEM) images were recorded using an FEI Tecnai G2 S-Twin with a field-emission gun operating at 200 kV. An electron paramagnetic resonance (EPR) spectrum was taken on the JES-FA200 electronic spin resonance spectrometer. The X-ray photoelectron spectra (XPS) were taken on a VG ESCALAB MK II electron spectrometer using Mg Kα (1200 eV) as the excitation source. The photoluminescence (PL) measurements were recorded with a Hitachi F-7000 spectrophotometer equipped with a 150 W xenon lamp as the excitation source. Photoluminescence quantum yields (QY) were measured directly by the absolute PL quantum yield (internal quantum efficiency) measurement system (C9920-02, Hamamatsu Photonics K. K., Japan), which comprises an excitation light source of a Xe lamp, a monochromator, an integrating sphere capable of nitrogen gas flow, and a CCD spectrometer for detecting the whole spectral range simultaneously. The luminescence decay curves were obtained from a Lecroy Wave Runner 6100 Digital Oscilloscope (1 GHz) using a tunable laser (pulse width = 4 ns, gate = 50 ns) as the excitation source (Contimuum Sunlite OPO). All the measurements were performed at room temperature (RT).

RESULTS AND DISCUSSION

Phase Identification and Morphology. Figure 1 shows the experimental, calculated, and difference results of the XRD refinement of $Ca_2Ba_3(PO_4)_3Cl$ at room temperature. The initial structural model was constructed with crystallographic data previously reported for $Ba_5(PO_4)_3Cl$ (ICSD #8191). The lattice parameters, zero point error, scale factor, and background are refined. Profile parameters (i.e., U, V, W) were refined next. Structural parameters are refined including the atomic coordinates and isotropic atomic displacement parameters for all the atoms. Here, we particularly assume that Ca ion substitutes for Ba1 at 4f sites, as shown in the crystal structure in Figure 1b. All of the observed peaks satisfy the reflection condition (R_{min} = 5.2%). The refinement results confirmed that the single-phase nature of the $Ca_2Ba_3(PO_4)_3Cl$ is related to the natural apatite (space group $P6_3/m$) with unit cell parameters $a = b$ = 10.045165 Å, c = 7.494675 Å, and V = 654.934 Å^3. Figure 2 presents the representative XRD patterns of the different

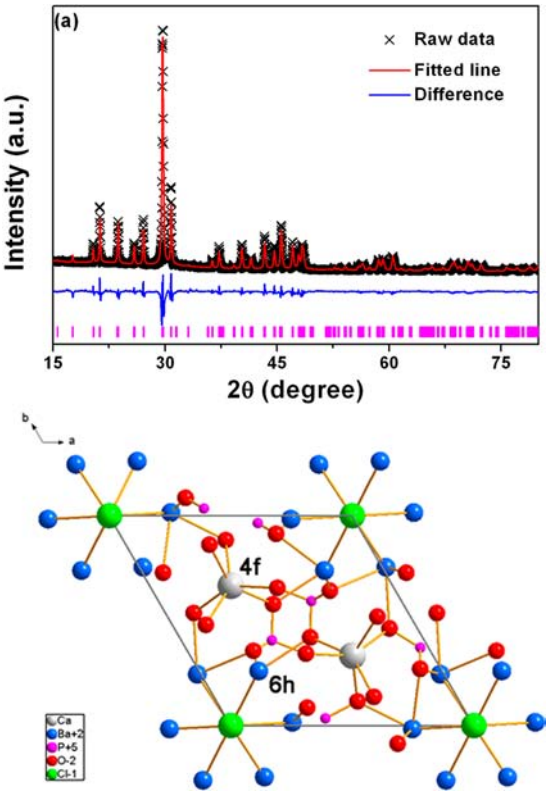

Figure 1. (a) Rietveld refinement of powder XRD profile of $Ca_2Ba_3(PO_4)_3Cl$. (b) Schematic crystal structure of $Ca_2Ba_3(PO_4)_3Cl$ with one unit cell.

dx.doi.org/10.1021/ic3025759 | Inorg. Chem. 2013, 52, 3102–3112

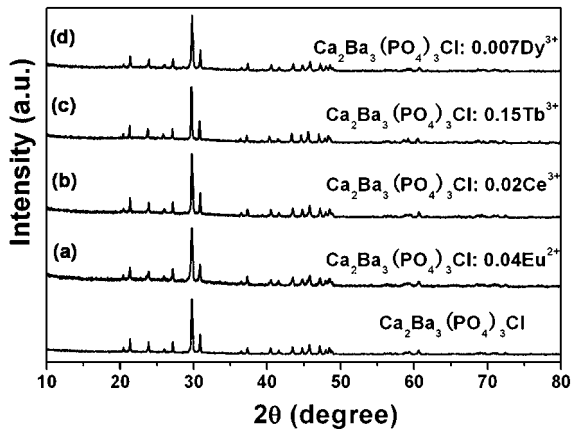

Figure 2. The representative XRD patterns of (a) $Ca_2Ba_3(PO_4)_3Cl$:0.04Eu^{2+}, (b) $Ca_2Ba_3(PO_4)_3Cl$:0.02Ce^{3+}, (c) $Ca_2Ba_3(PO_4)_3Cl$:0.15Tb^{3+}, and (d) $Ca_2Ba_3(PO_4)_3Cl$:0.007Dy^{3+} samples. The XRD pattern of $Ca_2Ba_3(PO_4)_3Cl$ is for comparison.

doping contents of Eu^{2+}, Ce^{3+}, Tb^{3+}, and Dy^{3+} ion doped $Ca_2Ba_3(PO_4)_3Cl$ samples. No impurity peaks are observed, and all the reflections can be well indexed to an apatite structure of $Ca_2Ba_3(PO_4)_3Cl$, indicating that the obtained samples are single phase and the doped Ln (Ln = Eu^{2+}, Ce^{3+}, Tb^{3+}, or Dy^{3+}) ion does not cause any significant change. It is worth noting that as formulated in this paper, the compositions $Ca_2Ba_3(PO_4)_3Cl$:Ce^{3+}/Tb^{3+}/Dy^{3+} are not charge balanced, having a slight excess of positive charge because of Ce^{3+}/Tb^{3+}/Dy^{3+} substituting Ca^{2+}. The structure offers many mechanisms to compensate this excess charge, and the most obvious one is the slight off-stoichiometry between Cl and O, with a slight excess of the latter. Since the experimental techniques we have employed here, namely, X-ray diffraction data, Rietveld refinement of powder, optical properties, etc., are not sensitive to substitutions at this level, we present the formula $Ca_2Ba_3(PO_4)_3Cl$:Ce^{3+}/Tb^{3+}/Dy^{3+} for the compounds as written, in preference to speculation.[3a] As the compound $Ca_2Ba_3(PO_4)_3Cl$ is isostructural with the apatite structure, there are two kinds of cationic site in the $Ca_2Ba_3(PO_4)_3Cl$ host, which are labeled $M_{(I)}$ and $M_{(II)}$ with local symmetry C_3 and C_S, repectively.[11] The $M_{(I)}$ site has a 3-fold symmetry C_3 axis parallel to the z axis and is nine-coordinate with oxygen ions. In the $M_{(II)}$ site, the cationic ion is 7-fold coordinate with C_S point group symmetry. Six oxygen ions and one chlorine ion act as the ligands. Owing to this structure, $Ca_2Ba_3(PO_4)_3Cl$ with the apatite structure has great capacity to form a solid solution and to accept several substitutes.[11−14]

The morphology of the $Ca_2Ba_3(PO_4)_3Cl$ sample is presented by the SEM and TEM images, as shown in Figure S1(Supporting Information). It seems that the sample is composed of particles with sizes ranging from 1 to 5 μm. The serious aggregated crystallites are attributed to the high temperature annealing process. The fine structures of $Ca_2Ba_3(PO_4)_3Cl$ were studied by the HRTEM technique. The insert in Figure S1 is its corresponding HRTEM image, in which the lattice fringes with a d spacing of 0.303 nm correspond to the distance of the (112) plane of $Ca_2Ba_3(PO_4)_3Cl$. The result further confirms the presence of a highly crystalline $Ca_2Ba_3(PO_4)_3Cl$ phase after being annealed at 1000 °C, agreeing well with the XRD results. It is worth noting that the dopants, such as Ce^{3+}, Eu^{2+}, Tb^{3+} and Dy^{3+} ions in our experiment do not influence the morphology of $Ca_2Ba_3(PO_4)_3Cl$, which will not shown here.

Photoluminescence Properties. *Undoped $Ca_2Ba_3(PO_4)_3Cl$.* Under UV-light irradiation, a broad band emission centered in the blue region can be observed when $Ca_2Ba_3(PO_4)_3Cl$ powder is exposed to a reducing atmosphere (90%N_2/10%H_2). Figure 3 (line a) shows the photo-

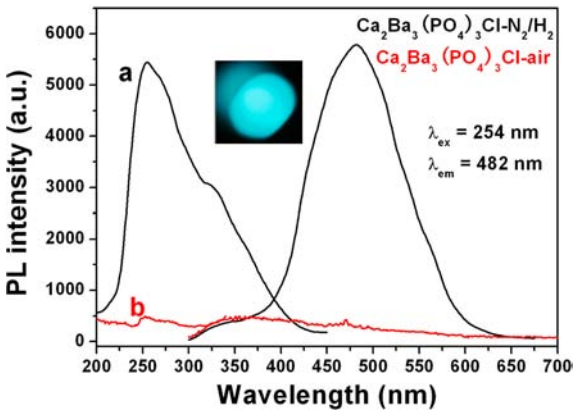

Figure 3. Photoluminescence excitation and emission spectra of (a) $Ca_2Ba_3(PO_4)_3Cl$-90%N_2/10%H_2 and (b) $Ca_2Ba_3(PO_4)_3Cl$-air samples. The inset shows the digital luminescence photograph of the $Ca_2Ba_3(PO_4)_3Cl$-90%N_2/10%H_2 samples excited at 254 nm in a UV box.

luminescence excitation and emission spectra of the $Ca_2Ba_3(PO_4)_3Cl$-90%N_2/10%H_2 sample. We can see that the $Ca_2Ba_3(PO_4)_3Cl$-90%N_2/10%H_2 sample shows a strong emission consisting of a broad band (360−600 nm) with a maximum at 482 nm. The corresponding excitation spectrum includes two broad bands: a strong broad band from 200 to 320 nm with a maximum at 254 nm and a weak band from 320 to 425 nm. However, no emission was observed for $Ca_2Ba_3(PO_4)_3Cl$ powder sintered in the air, as shown in Figure 3 (line b). In addition, the experiments were performed as a function of reaction time and reducing gas flow rate. However, the results indicate that the changes of the reducing time and gas flow rate have no effect on the luminescence property. Since neither the Ca^{2+}/Ba^{2+} nor the PO_4^{3-} group is able to show luminescence, the observed blue luminescence from the $Ca_2Ba_3(PO_4)_3Cl$-90%N_2/10%H_2 sample may be related to some impurities and/or defects in the host lattice. Since no literature concerning the self-activated luminescence of the $Ca_2Ba_3(PO_4)_3Cl$ sample can be found, we can only explain this luminescence phenomenon according to the existing models for other materials. Zhang et al. have reported that there exists defect emission in the $Ca_5(PO_4)_3F$ host, which is arising from $CO_2^{\bullet-}$ radical impurities in the crystal lattice, and the $CO_2^{\bullet-}$ radical is produced by trisodium citrate (Cit^{3-}) in the prepared process.[15] In our experiment, citric acid is also added as a chelating agent. In order to exclude the influence of Cit^{3-}, the $Ca_2Ba_3(PO_4)_3Cl$-SS sample was prepared via a solid state reaction with $CaCl_2$, $BaCl_2{\cdot}2H_2O$, and $(NH_4)H_2PO_4$ as raw materials. The obtained $Ca_2Ba_3(PO_4)_3Cl$-SS powder was also exposed to a reducing atmosphere (90%N_2/10%H_2) under the same conditions. Figure S2 (Supporting Information) shows the photoluminescence excitation and emission spectra of the $Ca_2Ba_3(PO_4)_3Cl$-SS sample treated in the reducing atmosphere. It can be seen that a broad band emission was also observed

dx.doi.org/10.1021/ic3025759 | Inorg. Chem. 2013, 52, 3102−3112

similar to the product prepared by the sol−gel method. This result indicates that the luminescence of $Ca_2Ba_3(PO_4)_3Cl$ is not due to the citric acid. The luminescence decay curve of the $Ca_2Ba_3(PO_4)_3Cl$-90%N_2/10%H_2 sample with blue emission shows a multiexponential decay ($I_{(t)} = A_1 \exp(-t/\tau_1) + A_2 \exp(-t/\tau_2) + I_0$) with a fast initial decay followed by a slow tail as shown in Figure S3 (Supporting Information), in which a dominant long decay time of 54.54 μs and a shorter decay time of 2.74 μs were observed. The fact that we observe at least two distinct luminescence decay processes points to two separate structural defect locations where luminescence occurs in these materials. Note that a very similar situation was reported by Vogt and Park,[8] who show that a family of anion ordered oxyfluorides with the general composition $Sr_{3-x}A_xMO_4F$ (A = Ca, Ba; M = Ga, Al) develop defect structures during exposure to reducing gases. They suggest that defects responsible for converting them into nonstoichiometric self-activating phosphors with the general formula $Sr_{3-x}A_xMO_{4-\alpha}F_{1-\delta}$, which means two different defect clusters exist, one in the Sr_2F^{3+} layer, the other in the $Sr(AlO_4)^{3-}$ block. The possible luminescence mechanism of the $Ca_2Ba_3(PO_4)_3Cl$ sample treated under reducing conditions may be also attributed to two defect clusters in the host lattice, one in A-O (A = Ca/Ba) groups, the other in A-Cl (A = Ca/Ba) groups. Figure S4 (Supporting Information) shows the EPR spectrum of the $Ca_2Ba_3(PO_4)_3Cl$-90%N_2/10%H_2 sample. It can be observed that the $Ca_2Ba_3(PO_4)_3Cl$-90%N_2/10%H_2 sample presents obvious EPR bands. However, the $Ca_2Ba_3(PO_4)_3Cl$-air sample exhibits no EPR signal (not shown here). This indicates that the paramagnetic defects relating to the luminescence property exist in the $Ca_2Ba_3(PO_4)_3Cl$-90%N_2/10%H_2 sample.[7,8]

$Ca_2Ba_3(PO_4)_3Cl:Eu^{2+}/Ce^{3+}$. Broad band emitting rare earth ions Eu^{2+} and Ce^{3+} have been widely studied due to their unique emission properties, combining a broad emission spectrum, relatively small Stokes shift, and short decay times.[16−19] In our experiment, Eu^{2+} and Ce^{3+} ions are doped in the $Ca_2Ba_3(PO_4)_3Cl$ host and exhibit excellent luminescence properties.

The photoluminescence excitation and emission spectra of the $Ca_2Ba_3(PO_4)_3Cl$:0.04Eu^{2+} sample are shown in Figure 4a. Monitored with 490 nm, the excitation spectrum consists of a broad band from 200 to 450 nm with a maximum at 274 nm due to transitions of Eu^{2+} from the $4f^7$ ground state to the $4f^65d^1$ excited state.[20] The Eu^{2+} ions have many excited states, and consequently, they show unresolved broad excitation spectra. The excitation spectrum shows that the excitation wavelength can extend from 200 to 450 nm, which nearly covers the whole UV region. Thus, it can be pumped by an InGaN-based UV chip and might be used in white LEDs. Under 274 nm UV-light irradiation, $Ca_2Ba_3(PO_4)_3Cl$:0.04Eu^{2+} shows a strong, asymmetric, broad band from 400 to 600 nm with a maximum wavelength at about 490 nm, which all can be ascribed to the $4f^65d^1 \rightarrow 4f^7$ allowed transition of Eu^{2+}. The asymmetric emission band from 400 to 600 nm can be deconvoluted into two Gaussian components peaking at 509 nm (I_1) and 466 nm (I_2), respectively, which are shown in Figure 4b. The two emission bands are due to the fact that there is more than one emitting center in the $Ca_2Ba_3(PO_4)_3Cl$ lattice. As discussed earlier, there are two cations available for Eu^{2+}: the $M_{(I)}$ and the $M_{(II)}$ sites.[15,21] According to the equation $E(cm^{-1}) = Q^*[1 - (V/4)^{1/V} \times 10^{-(nEar)/80}]$,[22] it can be deduced that the first band centered at 509 nm is due to the $4f^65d^1 \rightarrow 4f^7$ emission of the Eu^{2+} ion occupying the $M_{(II)}$ site with C_S symmetry and seven-coordination, and the second band centered at 466 nm is attributed to the $4f^65d^1 \rightarrow 4f^7$ emission of the Eu^{2+} ion occupying the $M_{(I)}$ site with C_3 symmetry and nine-coordination. The CIE chromaticity coordinates for the $Ca_2Ba_3(PO_4)_3Cl$:0.04Eu^{2+} sample under 274 nm UV excitation are (0.163, 0.344), and its luminescence photograph is shown in Figure 4a. It can be seen that the Eu^{2+} doped $Ca_2Ba_3(PO_4)_3Cl$ sample shows bright cyan emission. Generally speaking, the defect is not in favor of luminescence. As the $Ca_2Ba_3(PO_4)_3Cl$:0.04Eu^{2+} sample has similar emission properties to the $Ca_2Ba_3(PO_4)_3Cl-N_2/H_2$ sample, their PL properties are studied under the same test conditions, shown in Figure S5 (Supporting Information). It can be seen that the $Ca_2Ba_3(PO_4)_3Cl$:0.04Eu^{2+} sample has a wider excitation range, and its emission intensity is far higher than the defect luminescence. So the defect luminescence in the $Ca_2Ba_3(PO_4)_3Cl:Eu^{2+}$ sample can be ignored. The results confirmed that the cyan emission really comes from the $4f^65d^1 \rightarrow 4f^7$ transition of Eu^{2+} ions. Moreover, the PL emission spectrum in the full range (300−800 nm) only shows the broad emission from the $4f^65d^1 \rightarrow 4f^7$ transition of Eu^{2+} ions, indicating that there is no change of oxidation state of Eu^{2+} ions. Figure S6a (Supporting Information) shows the variation of PL intensity of $Ca_2Ba_3(PO_4)_3Cl:xEu^{2+}$ samples with the Eu^{2+} concentration (x) under 318 nm UV excitation. At first, the PL emission intensity of Eu^{2+} increases with the increase of its concentration (x), reaching a maximum value at x = 0.04 and

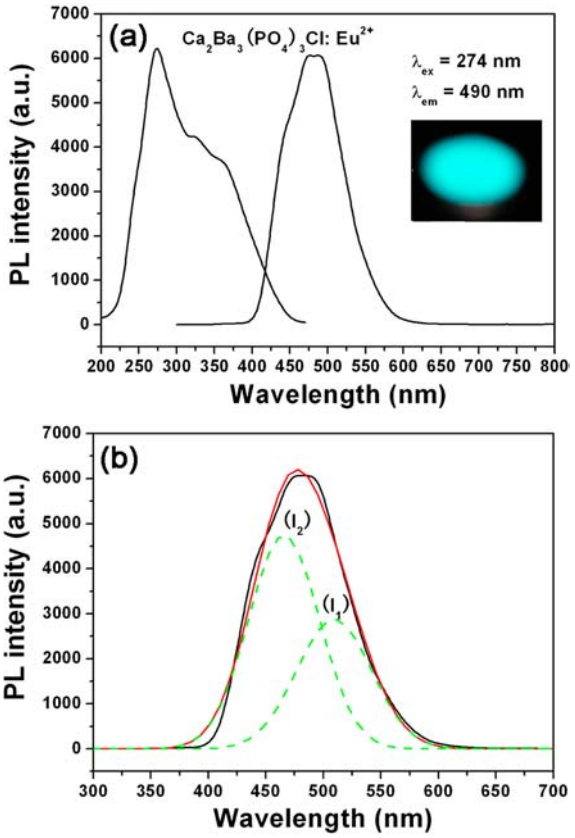

Figure 4. (a) Typical photoluminescence excitation and emission spectra of the $Ca_2Ba_3(PO_4)_3Cl$:0.04Eu^{2+} sample. The inset shows its digital luminescence photograph excited at 254 nm in a UV box. (b) The emission spectrum of $Ca_2Ba_3(PO_4)_3Cl$:0.04Eu^{2+} under λ_{ex} = 274 nm and its Gaussian components at 509 nm (I_1), 466 nm (I_2), respectively.

dx.doi.org/10.1021/ic3025759 | Inorg. Chem. 2013, 52, 3102−3112

then decreasing with a further increase of its concentration (x) due to the concentration quenching effect. In general, the concentration quenching of luminescence is due to the energy migration among the activator ions at the high concentrations. In the energy migration process, the excitation energy will be lost at a killer or quenching site, resulting in the decrease of luminescence intensity.[23] It was found that the energy transfer between inequivalent Eu^{2+} centers occurred at a Eu^{2+} concentration above 1%, which is consistent with the fact that the optimum concentration of Eu^{2+} is 4%.[24] The PL quantum efficiencies for the $Ca_2Ba_3(PO_4)_3Cl$:0.04Eu^{2+} sample can reach up to 72% and 61% under the excitation of 274 and 365 nm, respectively. The decay curves of Eu^{2+} in $Ca_2Ba_3(PO_4)_3Cl$:xEu^{2+} samples are well fitted with a double-exponential function, consistent with the fact that there exist two kinds of Eu^{2+} luminescence center. Figure S6b (Supporting Information) gives the decay curve of the representative $Ca_2Ba_3(PO_4)_3Cl$:0.04Eu^{2+} sample and the lifetimes of the Eu^{2+} ion in $Ca_2Ba_3(PO_4)_3Cl$:xEu^{2+} (x = 0.01−0.08) samples with different Eu^{2+} doping concentrations. As the Eu^{2+} doping concentration increases, the lifetime of Eu^{2+} gradually decreases, which may be mainly due to the energy transfer between two adjacent Eu^{2+} ions. However, the energy transfer is not the only factor. As the ion radius of Eu^{2+} and Ca^{2+} is different, the crystal structure distortion becomes more serious with an increase in the Eu^{2+} doping concentration, which would quench the luminescence and cause the lifetime to shorten.

Figure 5 shows the photoluminescence excitation and emission spectra of $Ca_2Ba_3(PO_4)_3Cl$:0.016Ce^{3+} monitored

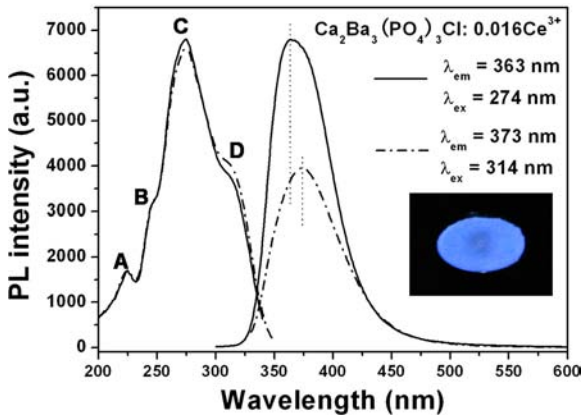

Figure 5. Photoluminescence excitation and emission spectra of the $Ca_2Ba_3(PO_4)_3Cl$:0.016Ce^{3+} sample. The inset shows its digital luminescence photograph excited at 254 nm in a UV box.

with different wavelengths and its luminescence photograph under the excitation of the 254 nm UV lamp. It can be seen that the Ce^{3+} doped $Ca_2Ba_3(PO_4)_3Cl$ sample exhibits bright blue emission due to the $5d^1 \rightarrow 4f^1$ transition of Ce^{3+}. It is noted that the emission spectra profiles are different when the phosphor is excited with different wavelength lights; the excitation spectra are also different under different wavelength light monitoring. The characteristic broad emission bands of Ce^{3+} are observed upon the excitation of both 274 and 314 nm. Their emission maxima are obviously different and are located at about ∼363 and ∼373 nm, respectively. The excitation spectra have identical profiles on the short-wavelength side (below ∼290 nm), containing three absorption bands marked A (∼ 224 nm), B (∼ 250 nm), and C (∼ 274 nm). However, the excitation spectrum recorded by monitoring the emission of 373 nm contains a stronger shoulder band D at ∼314 nm than that recorded by monitoring the emission of 363 nm. The profile differences of both emission spectra and excitation spectra are more distinct with the increasing concentration of Ce^{3+}. Figure S7a (Supporting Information) shows the excitation spectra of $Ca_2Ba_3(PO_4)_3Cl$:yCe^{3+} with y = 0.004, 0.016, and 0.10 by monitoring with the emission of 373 nm. These spectra were normalized to the intensities of their strongest absorptions. Compared with the excitation spectrum monitored with 363 nm, the PLE intensity of $Ca_2Ba_3(PO_4)_3Cl$:Ce^{3+} samples at 314 nm in the excitation spectrum monitored with 373 nm had an enhancement with respect to that at 274 nm. These indicate that the absorption bands A−D in Figure 5 derive from different Ce^{3+} sites. The profile changes in the emission and excitation spectra (Figures 5 and S7a) are attributed to the presence of two different Ce^{3+} luminescence centers. In addition, the full width at half maximum (about 100 nm, 10^5 cm^{-1}) of the $Ca_2Ba_3(PO_4)_3Cl$:Ce^{3+} sample is broader, which is also consistent with the result of two crystallographic positions for Ce^{3+} ions. Similar to Eu^{2+}, the two luminescence centers are related to the crystal structure of $Ca_2Ba_3(PO_4)_3Cl$, which provides two different sites for the cations in it, as discussed earlier, i.e., $M_{(I)}$ located at the 4f (C_3) site resulting in the emission at ∼360 nm and $M_{(II)}$ at the 6h (C_S) site resulting in the emission at ∼373 nm.[15,21,22] Furthermore, from the normalized emission spectrum in Figure S7b and c (Supporting Information), upon the 274 and 314 nm excitation, the emission maxima shift from ∼360 to ∼378 nm and from ∼370 to ∼390 nm, respectively, with the doping concentration increasing from 0.004 to 0.10. This may be a result from the entrance of more Ce^{3+} ions into 6h or 4f sites and the change of $Ca_2Ba_3(PO_4)_3Cl$ crystal field at a high doping concentration. Table S1 (Supporting Information) gives the absolute quantum yields of $Ca_2Ba_3(PO_4)_3Cl$:yCe^{3+} (y = 0.004, 0.012, 0.016, 0.03, 0.05, 0.07) samples. The highest quantum yield among the samples can reach 67% with the CIE chromaticity coordinates (0.166, 0.059).

The systems containing Ce ions always have the Ce^{3+}/Ce^{4+} redox system. X-ray photoelectron spectra (XPS) analysis[25,26] was carried out to understand the changes in the valence chemistry and binding energy of constituent elements. Figure S8 (Supporting Information) shows the deconvoluted XPS spectrum for Ce (3d) in the $Ca_{2-x}Ba_3(PO_4)_3Cl$:0.012Ce^{3+} sample. XPS results indicate that Ce is in mixed valence states of 3+ (880.40, 885.5, 898.81, 903.7 ± 0.7 eV) and 4+ (882.7, 888.96, 898.2, 901.3, 907, 916.7 ± 0.7 eV). In the figure, I_2, I_4, and I_7 peaks are attributed to Ce^{3+}, while I_1, I_3, I_5, I_6, and I_8 are the characteristic peaks of Ce^{4+} ions. A semiquantitative analysis of the integrated peak area can provide the concentration of Ce^{3+} ions. It can be calculated as[27]

$$[Ce^{3+}] = \frac{A_2 + A_4 + A_7}{\sum A_i}$$

where A_i is the integrated area for peak "i". The concentration of Ce^{3+} ions is calculated to be 36.8%.

$Ca_2Ba_3(PO_4)_3Cl$:Dy^{3+}/Tb^{3+}/Ce^{3+}, Tb^{3+}. Most trivalent rare earth ions (with Ce^{3+} as the major exception) yield a set of relatively narrow emission lines, due to internal $4f^n-4f^n$ transitions, which are hardly affected by the host compound. The host plays some role in the emissive properties of these

dx.doi.org/10.1021/ic3025759 | Inorg. Chem. 2013, 52, 3102−3112

4f−4f emitters, as it influences the relative strength of the emission lines (via selection rules associated with the local symmetry), the crystal field dependent splitting of the emission lines, and the quantum efficiency (through the presence of nonradiative pathways and the thermal quenching behavior). Dy^{3+} and Tb^{3+} ions, as trivalent rare earth ions, are always used as efficient yellow-white and blue-green light emissive activators, respectively.

Figure 6 shows the photoluminescence excitation and emission spectra of $Ca_2Ba_3(PO_4)_3Cl$:$m$$Dy^{3+}$. The emission

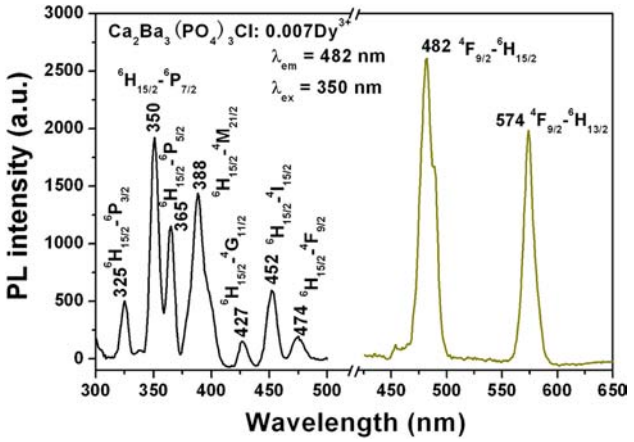

Figure 6. Photoluminescence excitation and emission spectra of the $Ca_2Ba_3(PO_4)_3Cl$:0.007Dy^{3+} sample.

spectrum of Dy^{3+} under the excitation of 350 nm wavelength is dominated by two main groups of emission in the blue region with a maximum at 482 nm and the yellow region with a maximum at 574 nm. These emissions correspond to the transitions from $^4F_{9/2}$ to $^6H_{15/2}$ and $^6H_{13/2}$ of Dy^{3+}, respectively.[28] There are a series of sharp excitation peaks from 300 to 500 nm in the excitation spectrum of $Ca_2Ba_3(PO_4)_3Cl$:$m$$Dy^{3+}$, which centered at 325, 350, 365, 388, 427, 452, and 474 nm come from 4f−4f transitions of the Dy^{3+} ion, which are attributed to $^6H_{15/2} \rightarrow {}^6P_{3/2}$, $^6H_{15/2} \rightarrow {}^6P_{7/2}$, $^6H_{15/2} \rightarrow {}^6P_{5/2}$, $^6H_{15/2} \rightarrow {}^4M_{21/2}$, $^6H_{15/2} \rightarrow {}^4G_{11/2}$, $^6H_{15/2} \rightarrow {}^4I_{15/2}$, and $^6H_{15/2} \rightarrow {}^4F_{9/2}$, respectively.[28,29] These excitation peaks are located at the excitation range of near-UV LED. So the $Ca_2Ba_3(PO_4)_3Cl$:Dy^{3+} sample may be suitable for near-UV LED devices. The PL intensity of the $Ca_2Ba_3(PO_4)_3Cl$:$m$$Dy^{3+}$ samples as a function of Dy^{3+} doping concentration is shown in Figure S9 (Supporting Information). The doping concentration of Dy^{3+} in the $Ca_2Ba_3(PO_4)_3Cl$ host is optimized in our experiments to be 0.7 mol %. Because the f−f absorption transitions of Dy^{3+} ions are forbidden transitions and are difficult to pump, the absolute quantum yield is low. In our experiment, the absolute quantum yield of the $Ca_2Ba_3(PO_4)_3Cl$:0.007Dy^{3+} sample only reaches 5% under the excitation of 355 nm.

For the Tb^{3+} ion, it has a low-energy ground state ^7F_j (j = 6, ..., 0) and excited states $^5D_3$ and $^5D_4$. Generally, with a low doping concentration of Tb^{3+} in the host matrix, the transitions of $^5D_3$ to ^7F_j dominate and produce the blue emissions. As the Tb^{3+} concentration increases, the cross relaxation from $^5D_3$ to $^5D_4$ occurs owing to the interaction between Tb^{3+} ions, which enhances the transitions of $^5D_4$ to ^7F_j with a green emission.[5] Figure 7 shows the PL spectra of the $Ca_2Ba_3(PO_4)_3Cl$:$z$$Tb^{3+}$ (z = 0.004, 0.012, 0.02) samples. The excitation spectra of the

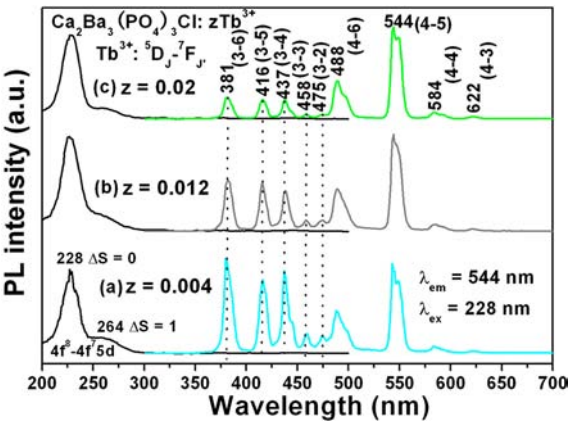

Figure 7. Photoluminescence excitation and emission spectra of $Ca_2Ba_3(PO_4)_3Cl$:$z$$Tb^{3+}$: (a) z = 0.004, (b) z = 0.012, and (c) z = 0.02.

three samples all show a strong absorption band from 200 to 250 nm with a maximum at 228 nm, and a weak band with a maximum at 264 nm. The former is related to the spin-allowed $4f^8 \rightarrow 4f^75d^1$ ($\Delta S = 0$) transition of Tb^{3+}, and the latter is due to the spin-forbidden $4f^8 \rightarrow 4f^75d^1$ ($\Delta S = 1$) transition. The energy difference of the two bands is about 5980 cm^{-1}, agreeing well with the value (6000 cm^{-1}) in the literature.[30] Besides the two absorption bands, there are some weak line absorptions in the excitation spectra from 300 to 500 nm, which are due to the intra-(4f) transitions of Tb^{3+} ions. Under 228 nm UV excitation, the emission spectra of the $Ca_2Ba_3(PO_4)_3Cl$:$z$$Tb^{3+}$ (z = 0.004, 0.012, 0.02) samples all consist of $^5D_{3,4} \rightarrow {}^7F_j$ transitions of Tb^{3+}, as shown in Figure 7. It can be seen that the emission spectra show different ratios between the $^5D_3$ and the $^5D_4$ emissions with changing Tb^{3+} concentrations. The emission spectrum for low Tb^{3+} concentration (z = 0.004; Figure 7a) consists of transitions from both the $^5D_3$ and $^5D_4$ levels. With an increase in the Tb^{3+} doping concentration (z = 0.012, 0.02; Figure 7b and c), the emissions from $^5D_3 \rightarrow {}^7F_j$ transitions are quenched gradually by the cross-relaxation process between neighboring Tb^{3+} ions. For the Tb^{3+} ion, the energy gap between the $^5D_3$ and $^5D_4$ levels is close to that between the $^7F_6$ and $^7F_0$ levels. As a result, if the Tb^{3+} concentration is high enough, the high energy level emission can be easily quenched in favor of the lower energy level emission, i.e., Tb^{3+} ($^5D_3$) + Tb^{3+} ($^7F_6$) → Tb^{3+} ($^5D_4$) + Tb^{3+} ($^7F_0$), accompanied by an enhancement of the emission from the $^5D_4$ level.[5] The PL intensity of the $Ca_2Ba_3(PO_4)_3Cl$:$z$$Tb^{3+}$ samples as a function of the Tb^{3+} doping concentration is shown in Figure S10 (Supporting Information). The doping concentration of Tb^{3+} in the $Ca_2Ba_3(PO_4)_3Cl$ host is optimized in our experiments to be 1.5 mol %. The concentration quenching effect is similar to that of Ce^{3+}, Eu^{2+}, and Dy^{3+} ions in the $Ca_2Ba_3(PO_4)_3Cl$ host.

Although the $Ca_2Ba_3(PO_4)_3Cl$:Tb^{3+} samples have excellent photoluminescence properties, the major problem with transferring these materials to LED applications is the lack of efficient, broad band excitation paths in the near-UV to blue part of the spectrum, where the 5d levels and some charge transfer states (CTS) are generally situated.[31,32] Moreover, the excitation spectrum can also be extended toward longer wavelengths by sensitizing through the appropriate addition of codopants. The Ce^{3+} ion is a well-known sensitizer for trivalent rare earth ions, especially for the Tb^{3+} ion, and the sensitizing effects depend strongly on the host lattices into

dx.doi.org/10.1021/ic3025759 | Inorg. Chem. 2013, 52, 3102−3112

which these ions are introduced.[33] In our experiment, the Tb^{3+} can also be well sensitized by Ce^{3+}, because the emission band of Ce^{3+} in the range of 300−450 nm overlaps with the excitation peaks of Tb^{3+} at 300−500 nm, as shown in Figure S11 (Supporting Information). A typical excitation and emission spectrum for a sample with composition $Ca_2Ba_3(PO_4)_3Cl$:0.015Ce^{3+},0.01Tb^{3+} is shown in Figure 8a.

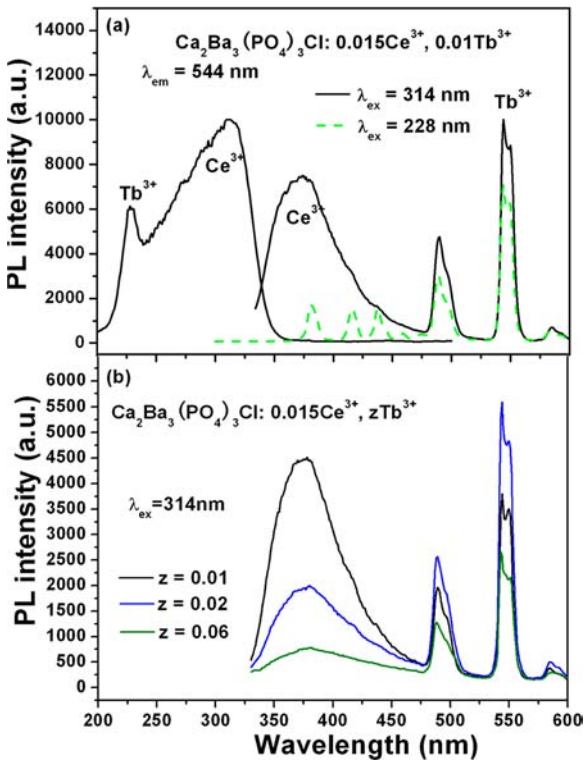

Figure 8. (a) Representative photoluminescence excitation and emission spectra of the $Ca_2Ba_3(PO_4)_3Cl$:0.015Ce^{3+},0.01Tb^{3+} sample. (b) The emission spectra of $Ca_2Ba_3(PO_4)_3Cl$:0.015Ce^{3+},$z$$Tb^{3+}$ (z = 0.01, 0.02, 0.06) samples as a function of Tb^{3+} doping concentration (z, mol %).

The excitation spectrum monitored with $^5D_4 \rightarrow {}^7F_5$ emission (544 nm) of the Tb^{3+} ion not only shows the absorption band of the Tb^{3+} ion at 228 nm but also the strong absorption broad band of the Ce^{3+} ion centered at 314 nm. The presence of the Ce^{3+} excitation band suggests energy transfer from Ce^{3+} to Tb^{3+}. Upon excitation into the Ce^{3+} absorption band, the $Ca_2Ba_3(PO_4)_3Cl$:0.015Ce^{3+},0.01Tb^{3+} sample simultaneously shows the blue emission of Ce^{3+} and the green emission of Tb^{3+}. In addition, upon excitation into the Ce^{3+} absorption band, the Ce^{3+} emission intensity of $Ca_2Ba_3(PO_4)_3Cl$:0.015Ce^{3+},$z$$Tb^{3+}$ (z = 0.01, 0.02, 0.06) samples (Figure 8b) decreases with the increase of Tb^{3+} concentration (z, mol %), which further confirms the existence of energy transfer from Ce^{3+} to Tb^{3+}. Table S1 (Supporting Information) gives the absolute quantum yields of $Ca_2Ba_3(PO_4)_3Cl$:0.015Ce^{3+},$z$$Tb^{3+}$ samples, which enhance with an increase in the Tb^{3+} doping concentration and reach a maximum at z = 0.02. In view of the $Ce^{3+} \rightarrow Tb^{3+}$ energy transfer in the $Ca_2Ba_3(PO_4)_3Cl$ host, the emission colors of $Ca_2Ba_3(PO_4)_3Cl$:0.015Ce^{3+},$z$$Tb^{3+}$ (z = 0, 0.005, 0.01, ..., 0.06) samples can be tuned from blue to green by changing the doping concentration of the Tb^{3+} ion.

In order to investigate the luminescence dynamics of the samples, we measured the PL decay curves of Ce^{3+} and then calculated the lifetime as well as energy transfer efficiencies from Ce^{3+} to Tb^{3+}, as shown in Figure S12 (Supporting Information). The decay curves of Ce^{3+} ions can be well fitted to a double-exponential function as $I_{(t)} = A_1 \exp(-t/\tau_1) + A_2\exp(-t/\tau_2) + I_{(0)}$ with a higher goodness fit shown in Figure S12a, which is due to the two different luminescence centers existing in the $Ca_2Ba_3(PO_4)_3Cl$ host, as mentioned previously.[15,21,22] The average luminescence lifetime of the Ce^{3+} ion is calculated to be 43.61 ns, using the formula $\tau = (A_1\tau_1^2 + A_2\tau_2^2)/(A_1\tau_1 + A_2\tau_2)$. With the increase of the Tb^{3+} doping concentration, the decay of the Ce^{3+} ions becomes faster and faster attributed to the energy transfer from the Ce^{3+} to Tb^{3+} ions, as shown in Figure S12b (Supporting Information). The average lifetimes of Ce^{3+} as a function of different Tb^{3+} concentrations were calculated and are shown in Figure S10c (black line, Supporting Information). In addition, the energy transfer efficiency from Ce^{3+} to Tb^{3+} was also investigated. Generally, the energy transfer efficiency from a sensitizer to activator can be expressed as the equation $\eta_T = 1 - \tau_S/\tau_{S0}$ (where τ_{S0} and τ_S are the lifetime of the Ce^{3+} sensitizer in the absence and presence of Tb^{3+} ions, respectively).[34] The η_T from Ce^{3+} to Tb^{3+} increased with increasing Tb^{3+} doping concentrations, as shown in Figure S12c (olive line, Supporting Information). The above results indicate that the energy transfer from Ce^{3+} to Tb^{3+} is efficient.

Generally, there are two main aspects responsible for the resonant energy-transfer mechanism: one is exchange interaction and the other is multipolar interaction.[35] It is known that if energy transfer results from the exchange interaction, the critical distance between the sensitizer and activator should be shorter than 4 Å.[35] In many cases, concentration quenching is due to energy transfer from one activator to another until an energy sink in the lattice is reached.[36] The critical distance R_C for energy transfer from the Ce^{3+} to Tb^{3+} ions can be calculated using the concentration quenching method. According to Blasse,[37] the critical distance R_C can be expressed by

$$R_C = 2\left(\frac{3V}{4\pi X_C N}\right)^{1/3}$$

where N is the number of available sites for the dopant in the unit cell, X_C is the total concentration of Ce^{3+} and Tb^{3+}, and V is the volume of the unit cell. For the $Ca_2Ba_3(PO_4)_3Cl$ host, N = 10 and V = 654.934 Å^3. The critical concentration X_C, at which the luminescence intensity of Ce^{3+} is half of that with the absence of Tb^{3+}, is about 0.035. Therefore, the critical distance (R_C) of energy transfer was calculated to be about 15.29 Å. The radiative emission from Ce^{3+} prevails when $R_{Ce-Tb} > R_C$ and energy transfer from Ce^{3+} to Tb^{3+} dominates when $R_{Ce-Tb} < R_C$. This value is much longer than 4 Å, indicating little possibility of energy transfer via the exchange interaction mechanism. Thus, the energy transfer between the Ce^{3+} and Tb^{3+} ions mainly takes place via electric multipolar interactions. On the basis of Dexter's energy transfer expressions of multipolar interaction and Reisfeld's approximation, the following relation can be given as[35−37]

$$\frac{\eta_{S0}}{\eta_S} \propto C^{n/3} \quad (1)$$

where η_{S0} and η_S are the luminescence quantum efficiencies of Ce^{3+} in the absence and presence of Tb^{3+}, respectively, and C is

dx.doi.org/10.1021/ic3025759 | Inorg. Chem. 2013, 52, 3102−3112

the total doping concentration of the Ce^{3+} and Tb^{3+} ions; eq 1 with n = 6, 8, and 10 corresponds to dipole−dipole, dipole−quadrupole, and quadrupole−quadrupole interactions, respectively. The value of η_{S0}/η_S can be approximately estimated from the related ratio of the lifetime (τ_{S0}/τ_S). Thus, eq 1 can be represented by the following equation:

$$\frac{\tau_{S0}}{\tau_S} \propto C^{n/3} \tag{2}$$

The relationships of $\tau_{S0}/\tau_S \propto C^{n/3}$ are illustrated in Figure S13 (Supporting Information), in which a linear behavior was observed only when n = 8, implying that energy transfer from Ce^{3+} to Eu^{2+} occurs via a dipole−quadrupole interaction. Therefore, the electric dipole−quadrupole interaction predominates in the energy transfer mechanism from the Ce^{3+} and Tb^{3+} ions in the $Ca_2Ba_3(PO_4)_3Cl$ host. Considering the dipole−quadrupole interaction, the critical distance formula sensitizer to an acceptor is given by the spectral overlap method. Hence, R_C can be obtained from the formula[35−38]

$$R_c^8 = 3.024 \times 10^{12} \lambda_S^2 f_q \int \frac{f_S(E) F_A(E)}{E^4} \, dE \tag{3}$$

where f_q is the oscillator strength of the involved absorption transition of the acceptor (Tb^{3+}), λ_S (in Å) is the wavelength position of the emission of the sensitizer, E is the energy involved in the transfer (in eV), and $\int f_S(E)F^A(E)\, dE/E^4$ represents the spectral overlap between the normalized shapes of the Ce^{3+} emission $f_S(E)$ and the Tb^{3+} excitation $F_A(E)$, and in our case it is calculated to be about 0.031 eV^{-4}. However, the oscillator strength of the Tb^{3+} quadrupole transitions (f_q) has not yet been obtained.[39] It is suggested by Verstegen et al. that the ratio f_q/f_d is about 10^{-2} to 10^{-3} when f_d applies to a forbidden dipole transition.[40] Using λ_S = 3750 Å, $f_q = 10^{-2}$ to $10^{-3} f_d$, f_d of the Tb^{3+} transition is 0.3×10^{-6}, and the critical distance (R_C) is calculated to be 12.22−16.30 Å for the dipole−quadrupole interaction. This result is in good agreement with that obtained using the concentration quenching method, which further reveals that the mechanism of energy transfer from the Ce^{3+} to Tb^{3+} ions is mainly due to a dipole−quadrupole interaction.

Cathodoluminescence Properties. In order to explore the potential of the as synthesized $Ca_2Ba_3(PO_4)_3Cl:Eu^{2+}/Ce^{3+}/Dy^{3+}/Tb^{3+}$ samples to be used as CL materials, their CL properties have been investigated in detail. Figure 9 shows the representative CL spectrum of the $Ca_2Ba_3(PO_4)_3Cl:0.04Eu^{2+}$ sample. The samples with different Eu^{2+} ion doping concentrations have the same spectrum with the $Ca_2Ba_3(PO_4)_3Cl:0.04Eu^{2+}$ sample, and their CL spectra profiles are similar to their PL spectra. Under the low voltage electron beam excitation, the pure $Ca_2Ba_3(PO_4)_3Cl:0.04Eu^{2+}$ sample gives bright cyan emission, whose emission spectrum consists of a broad band (400−600 nm) centered at 490 nm due to the $4f^65d^1 \rightarrow 4f^7$ transition of Eu^{2+}. The cyan emission of $Ca_2Ba_3(PO_4)_3Cl:0.04Eu^{2+}$ can be determined by its luminescence photograph inserted in Figure 9 and its CIE coordinates (0.158, 0.292) calculated through its CL spectrum. It is known that the color gamut for FED phosphors is determined by the location of their CIE chromaticity coordinates, which are typically made up of a triangle enclosed by three CIE chromaticity coordinate points, namely, 0.647 and 0.343 for red $Y_2O_2S:Eu^{3+}$, 0.298 and 0.619 for green ZnS:Cu,Al, and 0.146 and 0.056 for blue ZnS:Ag.[41] Accordingly, some novel

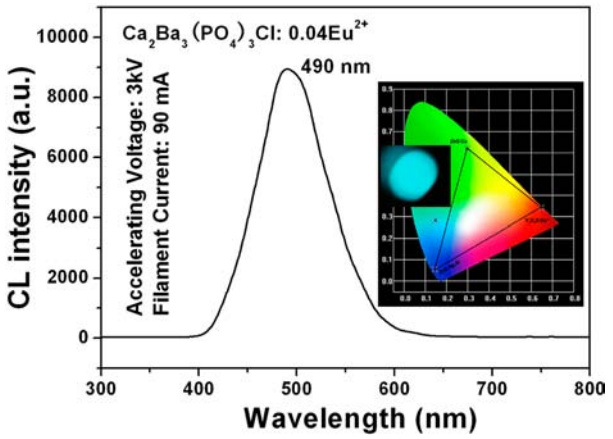

Figure 9. The typical cathodoluminescence (CL) spectrum of the $Ca_2Ba_3(PO_4)_3Cl:0.04Eu^{2+}$ sample; the inset shows its digital CL photograph and CIE chromaticity diagram.

phosphors with their CIE chromaticity coordinates located out of the above triangle area can enlarge the color gamut of those tricolor phosphors and could improve the display quality of full-color FEDs. As shown in the CIE coordinate diagram inserted in Figure 9, the $Ca_2Ba_3(PO_4)_3Cl:0.04Eu^{2+}$ sample just accords with that requirement. Accordingly, if the cyan light-emitting $Ca_2Ba_3(PO_4)_3Cl:0.04Eu^{2+}$ was added as an additional phosphor of the typical tricolor FED phosphors (as mentioned above), the chromaticity gamut and color saturation would be enhanced, which is favorable for improving the display quality of full-color FEDs.

For Ce^{3+} ion doped $Ca_2Ba_3(PO_4)_3Cl$ samples, their CL spectra are presented in Figure 10. Under the low voltage

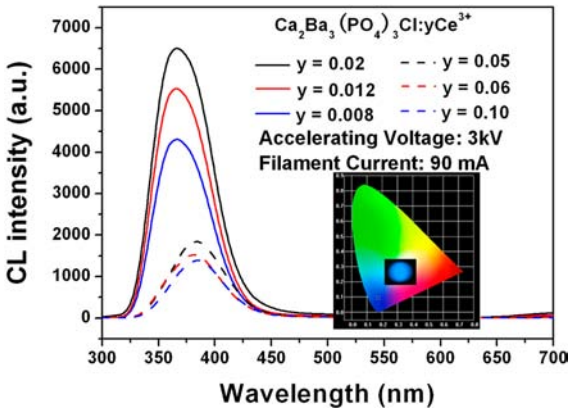

Figure 10. The typical CL spectra of the $Ca_2Ba_3(PO_4)_3Cl:yCe^{3+}$ (y = 0.008, 0.012, 0.02, 0.05, 0.06, 0.10) samples; the inset shows the digital CL photograph and CIE chromaticity diagram.

electron beam excitation, pure $Ca_2Ba_3(PO_4)_3Cl:yCe^{3+}$ (y = 0.008, 0.012, 0.02, 0.05, 0.06, 0.10) samples give a bright blue emission, whose emission spectrum consists of a broad band ranging from 320 to 450 nm due to the $5d^1 \rightarrow 4f^1$ transition of Ce^{3+}. The blue emission of $Ca_2Ba_3(PO_4)_3Cl:0.012Ce^{3+}$ can also be determined by its CIE coordinates (0.172, 0.094) calculated through its CL spectrum. Note that the samples with different Ce^{3+} ion doping concentrations have similar CL spectra profiles to their corresponding PL properties. This phenomenon further confirmed that there exist two cationic sites occupied by Ce^{3+} ions. With increasing the doping concentration of Ce^{3+},

dx.doi.org/10.1021/ic3025759 | Inorg. Chem. 2013, 52, 3102−3112

more Ce^{3+} ions substitute for the $M_{(II)}$ site in the $Ca_2Ba_3(PO_4)_3Cl$ host lattice, resulting in the longer wavelength emission.

For Dy^{3+} ion doped $Ca_2Ba_3(PO_4)_3Cl$ samples, they have strong cathodoluminescence intensities. Figure 11 shows the

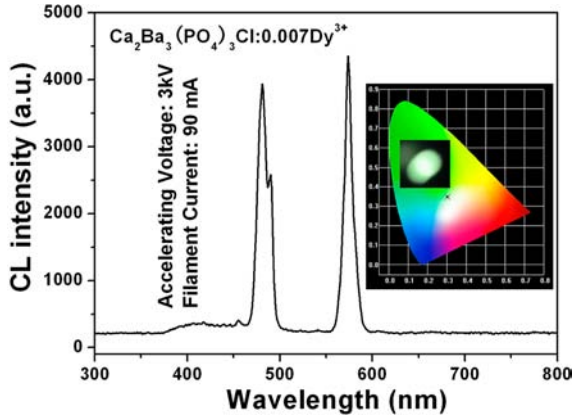

Figure 11. The typical CL spectra of the $Ca_2Ba_3(PO_4)_3Cl:0.007Dy^{3+}$. The inset shows its digital CL photograph and CIE chromaticity diagram.

CL spectrum and digital luminescence photograph of $Ca_2Ba_3(PO_4)_3Cl:0.007Dy^{3+}$. Similar to its PL spectrum, its CL spectrum is dominated by two main groups of emission in the blue region with a maximum at 482 nm and the yellow region with a maximum at 574 nm, and a yellow-green light was obtained.

Figure 12a illustrates the CL spectra of $Ca_2Ba_3(PO_4)_3Cl:zTb^{3+}$ (z = 0.004, 0.008, ..., 0.15) samples excited with a low voltage electron beam. The CL spectra consist of several emission peaks in the 380−700 nm range, and the blue emission coming from the $^5D_3 \rightarrow {}^7F_j$ (j = 2, 3...6) transitions of Tb^{3+} was more intense than the green emissions. Compared to their PL spectra, the emission peaks at 380, 420, and 440 nm were more prominent in the CL emission spectra. A similar phenomenon has been found in $LiAl_5O_8:Tb^{3+}$ and $Sr_3(PO_4)_2:Tb^{3+}$ phosphors.[42] It is well-known that the Tb ion can emit blue radiation if (a) the concentration quenching of the $^5D_3$ emission is low, (b) there is a weak multiphonon $^5D_3 \rightarrow {}^5D_4$ relaxation (a low phonon cutoff), and (c) the specific energy position of the $4f^7 \rightarrow 5d^1$ state minimum is lying above the $^5D_3$ state.[43] Usually, the $^5D_3$ state is sensitive to the concentration of the Tb^{3+} ions due to the cross relaxation process between $^7F_6 \rightarrow {}^7F_0$ and $^5D_3 \rightarrow {}^5D_4$ transitions, and therefore the blue emission is absent in materials with heavy Tb ion doping. However, the blue emitting $^5D_3$ level can be populated using high energy excitation such as cathode rays.[44] The $^5D_3 \rightarrow {}^7F_j$ transitions require assistance from low frequency phonons of the host matrix. In addition, the energy position of the $4f^75d^1$ must be blue-shifted to allow population of the $^5D_3$ state by a direct nonradiative relaxation process, as the configurational coordinate model shown in Figure 12b. Therefore, under electron beam excitation, the $Ca_2Ba_3(PO_4)_3Cl:Tb^{3+}$ samples show strong blue luminescence.

For purposes of comparison, the CL emission spectra of commercial blue phosphor $Y_2SiO_5:Ce^{3+}$ and the as prepared samples $Ca_2Ba_3(PO_4)_3Cl:Ce^{3+}$ and $Ca_2Ba_3(PO_4)_3Cl:Tb^{3+}$ are shown in Figure S14 (Supporting Information). The commercial blue phosphor $Y_2SiO_5:Ce^{3+}$ shows broadband

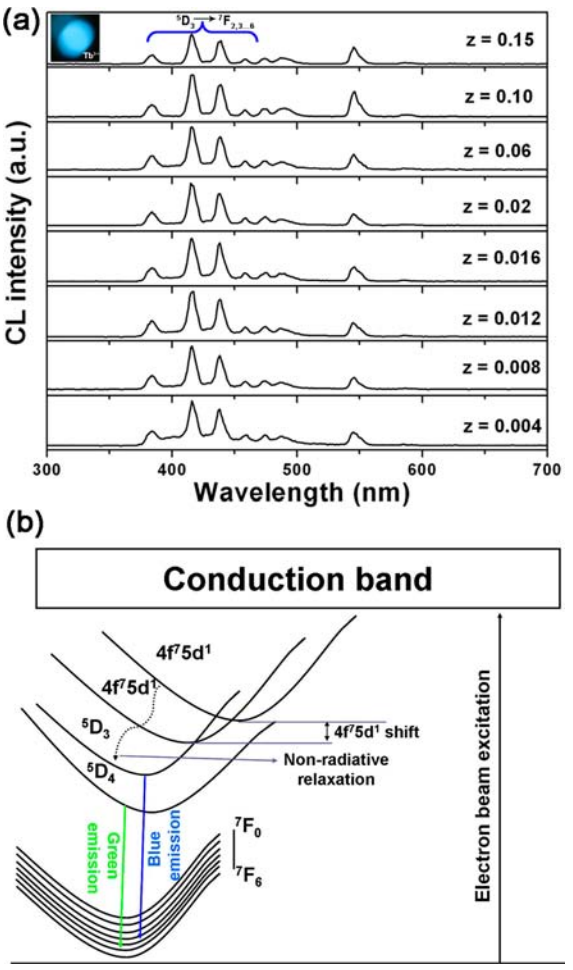

Figure 12. (a) CL spectra of $Ca_2Ba_3(PO_4)_3Cl:zTb^{3+}$ (z = 0.004, 0.008, ..., 0.15) samples (accelerating voltage = 3.0 kV, filament current = 90 mA). (b) The configurational coordinate model for the observed green and blue CL emission.

emission with maxima at 405 nm, and its corresponding CIE coordinates are determined to be (0.159, 0.063). Their luminescent photographs are also shown in Figure S14. For CL, the efficiency of a luminescent material includes the radiant efficiency (η) and the luminous efficiency (L, brightness),[5] which can be compared roughly by their emission peak areas (integrated luminescence intensity) and the CL intensity (in height), respectively. It can be seen from Figure S14 that the value of L for the as prepared sample $Ca_2Ba_3(PO_4)_3Cl:Ce^{3+}$ can reach up to 60% of the commercial phosphor $Y_2SiO_5:Ce^{3+}$. Moreover, the CIE coordinates (emission color) of $Ca_2Ba_3(PO_4)_3Cl:Ce^{3+}$ are more saturated than those of $Y_2SiO_5:Ce^{3+}$, which is more advantageous to full color field emission display.

The normalized CL emission intensities of $Ca_2Ba_3(PO_4)_3Cl:0.04Eu^{2+}$, $Ca_2Ba_3(PO_4)_3Cl:0.016Tb^{3+}$, and $Ca_2Ba_3(PO_4)_3Cl:0.007Dy^{3+}$ as a function of the accelerating voltage and the filament current are shown in Figure S15 (Supporting Information). When the filament current is fixed at 90 mA, the CL intensity increases on raising the accelerating voltage from 2.0 to 5.0 kV (Figure S15a). Similarly, under a 4.0 kV electron beam excitation, the CL intensity also increases with increasing the filament current from 84 to 92 mA (Figure S15b). There is no obvious saturation effect for the CL intensity of these samples with the increase of current density

dx.doi.org/10.1021/ic3025759 | Inorg. Chem. 2013, 52, 3102−3112

and accelerating voltage. The increase in CL brightness with an increase in electron energy and filament current is attributed to the deeper penetration of the electrons into the phosphor body and the larger electron-beam current density. The electron penetration depth can be estimated using the empirical formula $L\ (Å) = 250(A/\rho)(E/Z^{1/2})^n$, where $n = 1.2/(1 - 0.29 \log Z)$, A is the atomic or molecular weight of the material, ρ is the bulk density, Z is the atomic number or the number of electrons per molecule in the case of compounds, and E is the energy of the accelerating electron (eV).[45] The higher the accelerating voltage and filament current, the larger the energy of the accelerating electron and the deeper the penetration depth. For CL of the above samples, the Eu^{2+}, Tb^{3+}, and Dy^{3+} ions are excited by the plasma produced by the incident electrons. The deeper the electron penetration depth, the more plasma will be produced, which results in more activator ions being excited, and thus the CL intensity increases.

The degradation properties of phosphors are very important for FED application. Thus, we also investigated the degradation behavior of the as prepared samples under low voltage electron beam excitation. Figure S16 (Supporting Information) shows the decay behavior of the CL intensity of representative $Ca_2Ba_3(PO_4)_3Cl:0.04Eu^{2+}$, $Ca_2Ba_3(PO_4)_3Cl:0.016Tb^{3+}$, and $Ca_2Ba_3(PO_4)_3Cl:0.007Dy^{3+}$ samples under continuous electron beam bombardment with an accelerating voltage = 3.0 kV and a filament current = 90 mA. The CL peaks are almost the same as those before electron bombardment. However, the CL intensity of the studied sample continually decreases with prolonging the electron bombardment time. After continuous electron radiation for 60 min, the CL intensities of the $Ca_2Ba_3(PO_4)_3Cl:0.04Eu^{2+}$, $Ca_2Ba_3(PO_4)_3Cl:0.016Tb^{3+}$, and $Ca_2Ba_3(PO_4)_3Cl:0.007Dy^{3+}$ samples fell to 50%, 49%, and 30% of the initial value, respectively. This degradation of CL intensity may be due to the accumulation of carbon at the surface during electron bombardment.[46,47] The accumulation of graphitic carbon during electron-beam exposure at high current densities is a well-known effect. This carbon contamination will prevent low-energy electrons from reaching the phosphor grains and also exacerbate surface charging and thus lower the CL intensity. In addition, the stability of the as prepared Eu^{2+}, Tb^{3+}, and Dy^{3+} doped $Ca_2Ba_3(PO_4)_3Cl$ samples is much worse than other phosphors with apatite structure,[12,48] which may be due to the Cl ion in the $Ca_2Ba_3(PO_4)_3Cl$ host being unstable under the low voltage electron excitation and the defect structure forms. Moreover, after stopping the bombardment for a while, the CL intensity could not return to the initial value, indicating that permanent damage to the phosphor had occurred, which also results in the decrease of CL intensity.

CONCLUSIONS

In conclusion, self-activated $Ca_2Ba_3(PO_4)_3Cl$ and rare earth ion (Eu^{2+}/Ce^{3+}/Dy^{3+}/Tb^{3+}) activated $Ca_2Ba_3(PO_4)_3Cl$ phosphors have been prepared via a Pechini sol–gel method. Their PL and CL properties were investigated in detail. The undoped $Ca_2Ba_3(PO_4)_3Cl$ sample after being reduced shows broad band photoluminescence when excited by 254 nm UV light after being reduced, which may be due to two defect clusters in the host lattice, one in A-O (A = Ca/Ba) groups, the other in A-Cl (A = Ca/Ba) groups. With Eu^{2+} or Ce^{3+} ions doped into the $Ca_2Ba_3(PO_4)_3Cl$ host, broad band emissions with cyan light for Eu^{2+} ion and blue light for Ce^{3+} ion were observed under the UV light excited due to their respective 5d → 4f transitions. Moreover, the Dy^{3+} or Tb^{3+} ion doped $Ca_2Ba_3(PO_4)_3Cl$ phosphors presented line emissions due to their 4f → 4f transitions. In addition, Ce^{3+} as an effective sensitizer can also transfer energy to Tb^{3+}. The energy transfer mechanism of Ce^{3+} → Tb^{3+} has been demonstrated to be a resonant type via a dipole–quadrupole interaction. On the other hand, under the excitation of a low voltage electron beam, Eu^{2+}, Ce^{3+}, Dy^{3+}, or Tb^{3+} ion doped $Ca_2Ba_3(PO_4)_3Cl$ samples all show excellent cathodoluminescence properties. The CL spectra of $Ca_2Ba_3(PO_4)_3Cl:Eu^{2+}$, $Ca_2Ba_3(PO_4)_3Cl:Ce^{3+}$, and $Ca_2Ba_3(PO_4)_3Cl:Dy^{3+}$ samples are similar to their PL spectra. However, the CL properties for $Ca_2Ba_3(PO_4)_3Cl:Tb^{3+}$ samples are different from their PL properties, which are attributed to the different excitation mechanism. Our study on photoluminescence and cathodoluminescence properties of $Ca_2Ba_3(PO_4)_3Cl$ doped with rare earth ions (Eu^{2+}/Ce^{3+}/Dy^{3+}/Tb^{3+}) has shown that these materials might be candidates for solid-state lighting and field-emission displays.

ASSOCIATED CONTENT

Supporting Information

SEM, TEM, and HRTEM image; photoluminescence excitation and emission spectra; photoluminescence decay curve; EPR spectrum and XPS spectrum; PL intensity as a function of the activator doping concentration; dependence of the energy transfer efficiency (η_T) and the fluorescence lifetime of Ce^{3+} on Tb^{3+} content (z); dependence of τ_{S0}/τ_S of Ce^{3+} on $C^{6/3}$, $C^{8/3}$, and $C^{10/3}$; CL spectra and CL photograph; CL intensities as a function of accelerating voltage and filament current; and CL intensity as a function of the radiation time. This material is available free of charge via the Internet at http://pubs.acs.org.

AUTHOR INFORMATION

Corresponding Author

*E-mail: jlin@ciac.jl.cn.

Notes

The authors declare no competing financial interest.

ACKNOWLEDGMENTS

This project is financially supported by National Basic Research Program of China (2010CB327704), and the National Natural Science Foundation of China (NSFC 51172227 and 21221061). We thank Jun Lu (State Key Laboratory of Magnetism, Beijing National Laboratory for Condensed Matter Physics Institute of Physics, Chinese Academy of Sciences) for help in the samples characterization.

REFERENCES

(1) (a) Kuo, T.-W.; Chen, T.-M. *J. Electrochem. Soc.* **2010**, *157*, J216–J220. (b) Hirosaki, N.; Xie, R. J.; Inoue, K.; Sekiguchi, T.; Dierre, B.; Tamura, K. *Appl. Phys. Lett.* **2007**, *91*, 061101. (c) Wakefield, G.; Holland, E.; Dobson, P. J.; Hutchison, J. L. *Adv. Mater.* **2001**, *13*, 1557. (d) Choe, J. Y.; Ravichandran, D.; Blomquist, S. M.; Morton, D. C.; Kirchner, K. W.; Ervin, M. H.; Lee, U. *Appl. Phys. Lett.* **2001**, *78*, 3800.

(2) (a) Park, J. K.; Lim, M. A.; Kim, C. H.; Park, H. D.; Park, J. T.; Choi, S. Y. *Appl. Phys. Lett.* **2003**, *82*, 683–685. (b) Xie, R. J.; Hirosaki, N.; Mitomo, M.; Yamamoto, Y.; Suehiro, T. *J. Phys. Chem. B* **2004**, *108*, 12027–12031. (c) Setlur, A. A.; Heward, W. J.; Gao, Y.; Srivastava, A. M.; Chandran, R. G.; Shankar, M. V. *Chem. Mater.* **2006**, *18*, 3314–3322.

(3) (a) Im, W. B.; Brinkley, S.; Hu, J.; Mikhailovsky, A.; DenBaars, S. P.; Seshadri, R. *Chem. Mater.* **2010**, *22*, 2842–2849. (b) Li, Y. Q.; Delsing, A. C. A.; de With, G.; Hintzen, H. T. *Chem. Mater.* **2005**, *17*, 3242–3248. (c) Liu, Y. S.; Tu, D. T.; Zhu, H. M.; Li, R. F.; Luo, W. Q.; Chen, X. Y. *Adv. Mater.* **2010**, *22*, 3266–3271.

(4) (a) Vivero-Escoto, J. L.; Slowing, I. I.; Wu, C. W.; Lin, V. S. Y. *J. Am. Chem. Soc.* **2009**, *131*, 3462−3463. (b) Chen, F. H.; Gao, Q.; Ni, J. Z. *Nanotechnology* **2008**, *19*, 165103. (c) Li, Z.; Barnes, J. C.; Bosoy, A.; Stoddart, J. F.; Zink, J. I. *Chem. Soc. Rev.* **2012**, *41*, 2590−2605. (d) Park, Y. I.; Kim, J. H.; Lee, K. T.; Jeon, K. S.; Na, H. B.; Yu, J. H.; Kim, H. M.; Lee, N.; Choi, S. H.; Baik, S. I.; Kim, H.; Park, S. P.; Park, B. J.; Kim, Y. W.; Lee, S. H.; Yoon, S. Y.; Song, I. C.; Moon, W. K.; Suh, Y. D.; Hyeon, T. *Adv. Mater.* **2009**, *21*, 4467−4471. (e) Cao, L.; Wang, X.; Meziani, M. J.; Lu, F. S.; Wang, H. F.; Luo, P. J. G.; Lin, Y.; Harruff, B. A.; Veca, L. M.; Murray, D.; Xie, S. Y.; Sun, Y. P. *J. Am. Chem. Soc.* **2007**, *129*, 11318−11319.

(5) Blasse, G.; Grabmaier, B. C. *Luminescence Materials*; Springer-Verlag: New York, 1994; Chapters 4−5.

(6) (a) Tang, Y. S.; Hu, S. F.; Lin, C. C.; Bagkar, N. C.; Liu, R. S. *Appl. Phys. Lett.* **2007**, *90*, 151108. (b) Lee, S.; Sohn, K. *Opt. Lett.* **2010**, *35*, 1004−1006.

(7) (a) Kan, D.; Terashima, T.; Kanda, R.; Masuno, A.; Tanaka, K.; Chu, S.; Kan, H.; Ishizumi, A.; Kanemitsu, Y.; Shimakawa, Y.; Takano, M. *Nat. Mater.* **2005**, *4*, 816−819. (b) Kan, D.; Kanda, R.; Kanemitsu, Y.; Shimakawa, Y.; Takno, M.; Terashima, T.; Ishizumi, A. *Appl. Phys. Lett.* **2006**, *88*, 191916. (c) Zhang, C. M.; Lin, J. *Chem. Soc. Rev.* **2012**, *41*, 7938−7961.

(8) Park, S.; Vogt, T. *J. Phys. Chem. C* **2010**, *114*, 11576−11583.

(9) (a) Lin, J.; Yu, M.; Lin, C. K.; Liu, X. M. *J. Phys. Chem. C* **2007**, *111*, 5835−5845. (b) Serra, O. A.; Severino, V. P.; Calefi, P. S.; Cicillini, S. A. *J. Alloys Compd.* **2001**, *323*−*324*, 667−669. (c) Sousa Filho de, P. C.; Serra, O. A. *J. Fluoresc.* **2008**, *18*, 329−337.

(10) Larson, C.; Von Dreele, R. B. *Generalized Structure Analysis System (GSAS)*; Los Alamos National Laboratory Report LAUR 86−748, Los Alamos National Laboratory: Los Alamos, NM, 1994.

(11) (a) Sato, M.; Tanaka, T.; Ohta, M. *J. Electrochem. Soc.* **1994**, *141*, 1851−1855. (b) Sahoo, R.; Bhattacharya, S. K.; Debnath, R. *J. Solid State Chem.* **2003**, *175*, 218−225.

(12) Shang, M. M.; Geng, D. L.; Zhang, Y.; Li, G. G.; Yang, D. M.; Kang, X. J.; Lin, J. *J. Mater. Chem.* **2012**, *22*, 19094−19104.

(13) (a) Yu, J.; Guo, C. F.; Ren, Z. Y.; Bai, J. T. *Opt. Laser Technol.* **2011**, *43*, 762−766. (b) Ramesh, R.; Jagannathan, R. *J. Phys. Chem. B* **2000**, *104*, 8351−8360. (c) Xiu, Z. L.; Liu, S. W.; Ren, M.; Liu, J.; Pan, J.; Cui, X. P. *J. Alloys Compd.* **2006**, *425*, 261−263.

(14) (a) Zhang, Z.; Wang, J.; Zhang, M.; Zhang, Q.; Su, Q. *Appl. Phys. B: Laser Opt.* **2008**, *91*, 529−537. (b) Yoo, H. S.; Vaidyanathan, S.; Kim, S. W.; Jeon, D. Y. *Opt. Mater.* **2009**, *31*, 1555−1558.

(15) Zhang, C. M.; Huang, S. S.; Yang, D. M.; Kang, X. J.; Shang, M. M.; Peng, C.; Lin, J. *J. Mater. Chem.* **2010**, *20*, 6674−6680.

(16) Liu, L. H.; Xie, R. J.; Hirosaki, N.; Li, Y. Q.; Takeda, T.; Zhang, C. N.; Li, J. G.; Sun, X. D. *J. Am. Ceram. Soc.* **2010**, *93*, 2018−2023.

(17) (a) Kurushima, T.; Gundiah, G.; Shimomura, Y.; Mikami, M.; Kijima, N.; Cheetham, A. K. *J. Electrochem. Soc.* **2010**, *157*, J64−J68. (b) Xie, R. J.; Hirosaki, N.; Sakuma, K.; Kimura, N. *J. Phys. D: Appl. Phys.* **2008**, *41*, 144013.

(18) (a) Jing, H.; Guo, C. F.; Zhang, G. G.; Su, X. Y.; Yang, Z.; Jeong, J. H. *J. Mater. Chem.* **2012**, *22*, 13612−13618. (b) Liu, W. R.; Huang, C. H.; Wu, C. P.; Chiu, Y. C.; Yeh, Y. T.; Chen, T. M. *J. Mater. Chem.* **2011**, *21*, 6869−6874.

(19) (a) Smet, P. F.; Avci, N.; Poelman, D. *J. Electrochem. Soc.* **2009**, *156*, H243−H248. (b) Bachmann, V.; Ronda, C.; Oeckler, O.; Schnick, W.; Meijerink, A. *Chem. Mater.* **2009**, *21*, 316−325. (c) Xia, Q.; Batentschuk, M.; Osvet, A.; Winnacker, A.; Schneider, J. *Radiat. Meas.* **2010**, *45*, 350−352.

(20) Blasse, G.; Wanmaker, W. L.; Tervrugt, J. W.; Bril, A. *Philips Res. Rep.* **1968**, *23*, 189−200.

(21) Hughes, J. M.; Rakovan, J. *Mineral. Geochem.* **2002**, *48*, 1−12.

(22) (a) Van Uitert, L. G. *J. Lumin.* **1984**, *29*, 1−9. (b) Shang, M. M.; Li, G. G.; Geng, D. L.; Yang, D. M.; Kang, X. J.; Zhang, Y.; Lian, H. Z.; Lin, J. *J. Phys. Chem. C* **2012**, *116*, 10222−10231.

(23) (a) Lin, C. C.; Liu, R. S.; Tang, Y. S.; Hu, S. F. *J. Electrochem. Soc.* **2008**, *155*, J248−J251. (b) Bandi, V. R.; Jeong, J.; Shin, H.-J.; Jang, K.; Lee, H.-S.; Yi, S.-S.; Jeong, J. H. *Opt. Commun.* **2011**, *284*, 4504−4507. (c) Chan, T. S.; Lin, C. C.; Liu, R. S.; Xie, R. J.; Hirosaki, N.; Cheng, B. M. *J. Electrochem. Soc.* **2009**, *156*, J189−J191.

(24) Blasse, G. *J. Solid State Chem.* **1986**, *62*, 207−211.

(25) Deshpande, S.; Patil, S.; Kuchibhatla, S.; Seal, S. *Appl. Phys. Lett.* **2005**, *87*, 133113.

(26) Kumar, A.; Babu, S.; Karakoti, A. S.; Schulte, A.; Seal, S. *Langmuir* **2009**, *25*, 10998.

(27) Force, C.; Roman, E.; Guil, J. M.; Sanz, J. *Langmuir* **2007**, *23*, 4569.

(28) (a) Shang, M. M.; Li, G. G.; Kang, X. J.; Yang, D. M.; Lin, J. *J. Electrochem. Soc.* **2011**, *158*, H565−H571. (b) Li, G. G.; Peng, C.; Li, C. X.; Yang, P. P.; Hou, Z. Y.; Fan, Y.; Cheng, Z. Y.; Lin, J. *Inorg. Chem.* **2010**, *49*, 1449−1457.

(29) Jayasimhadri, M.; Ratnam, B. V.; Jang, K.; Lee, H. S.; Chen, B. j.; Yi, S.-S.; Jeong, J.-H.; Moorthy, L. R. *J. Am. Ceram. Soc.* **2010**, *93*, 494−499.

(30) Geng, D. L.; Li, G. G.; Shang, M. M.; Yang, D. M.; Zhang, Y.; Cheng, Z. Y.; Lin, J. *J. Mater. Chem.* **2012**, *22*, 14262−14271.

(31) Chen, W. P.; Liang, H. B.; Ni, H. Y. *J. Electrochem. Soc.* **2010**, *157*, J159−J163.

(32) Sivakumar, V.; Varadaraju, U. V. *Electrochem. Solid-State Lett.* **2006**, *9*, H35−H38.

(33) (a) Zhang, G.; Wang, J.; Chen, Y.; Su, Q. *Opt. Lett.* **2010**, *35*, 2382−2384. (b) Ghosh, P.; Kar, A.; Patra, A. *Nanoscale* **2010**, *2*, 1196−1202.

(34) (a) Yang, W. J.; Chen, T. M. *Appl. Phys. Lett.* **2006**, *88*, 101903. (b) Kar, A.; Datta, A.; Patra, A. *J. Mater. Chem.* **2010**, *20*, 916−922. (c) Paulose, P. I.; Jose, G.; Thomas, V.; Unnikrishnan, N. V.; Warrier, M. K. R. *J. Phys. Chem. Solids* **2003**, *64*, 841−846.

(35) Reisfeld, R.; Greenberg, E.; Velapoldi, R.; Barnett, B. *J. Chem. Phys.* **1972**, *56*, 1698−1705.

(36) Dexter, D. L. *J. Chem. Phys.* **1953**, *21*, 836−850.

(37) Blasse, G. *Philips Res. Rep.* **1969**, *24*, 131−144.

(38) Guo, N.; Huang, Y. J.; You, H. P.; Yang, M.; Song, Y. H.; Liu, K.; Zheng, Y. H. *Inorg. Chem.* **2010**, *49*, 10907−10913.

(39) (a) Huang, Y. J.; You, H. P.; Jia, G.; Song, Y. H.; Zheng, Y. H.; Yang, M.; Liu, K.; Guo, N. *J. Phys. Chem. C* **2010**, *114*, 18051−18058. (b) Huang, C. H.; Kuo, T. W.; Chen, T. M. *ACS Appl. Mater. Interfaces* **2010**, *2*, 1395−1399.

(40) Vestegen, J. M. P. J.; Sommerdijk, J. L.; Verriet, G. J. *J. Lumin.* **1973**, *6*, 425−431.

(41) Li, G. G.; Zhang, X.; Peng, C.; Shang, M. M.; Geng, D. L.; Cheng, Z. Y.; Lin, J. *J. Mater. Chem.* **2011**, *21*, 6477−6479.

(42) (a) Pitale, S. S.; Kumar, V.; Nagpure, I. M.; Ntwaeaborwa, O. M.; Coetsee, E.; Swart, H. C. *J. Appl. Phys.* **2011**, *109*, 013105. (b) Nagpure, I. M.; Pitale, S. S.; Coetsee, E.; Ntwaeaborwa, O. M.; Terblans, J. J.; Swart, H. C. *Appl. Surf. Sci.* **2011**, *257*, 10147−10155.

(43) Shinoya, S.; Yen, W. M. *Phosphor Handbook*; CRC: Boca Raton, FL, 1999.

(44) Brandstadter, I. J.; Reisfeld, R. S.; Larach, S. *Solid State Commun.* **1972**, *11*, 1235−1238.

(45) Feldman, C. *Phys. Rev.* **1960**, *117*, 455−459.

(46) Xu, X. G.; Chen, J.; Deng, S. Z.; Xu, N. S.; Lin, J. *J. Vac. Sci. Technol. B* **2010**, *28*, 490−494.

(47) Zhang, M. C.; Wang, X. J.; Ding, H.; Li, H. L.; Pan, L. K.; Sun, Z. *Int. J. Appl. Ceram. Technol.* **2011**, *8*, 752−758.

(48) Li, G. G.; Zhang, Y.; Geng, D. L.; Shang, M. M.; Peng, C.; Cheng, Z. Y.; Lin, J. *ACS Appl. Mater. Interfaces* **2012**, *4*, 296−305.